# INDIVIDUAL BLADE CONTROL EFFECTS ON BLADE-VORTEX INTERACTION NOISE

Stephen M. Swanson
Sterling Software, Inc.
Palo Alto, California

Stephen A. Jacklin
NASA Ames Research Center
Moffett Field, California

Achim Blaas
ZF Luftfahrttechnik, GmbH
Germany

Roland Kube
Institute of Flight Mechanics (DLR)
Braunschweig, Germany

Georg Niesl
Eurocopter Deutschland
Munchen, Germany

## Abstract

A full-scale wind tunnel test was conducted in the 40- by 80-Foot Wind Tunnel at NASA Ames Research Center to evaluate the effects of individual blade control on blade-vortex interaction noise. This international joint program involved NASA Ames Research Center, U.S. Army Aeroflightdynamics Directorate, ZF Luftfahrttechnik, DLR and Eurocopter Deutschland. A four-bladed BO 105 rotor system was mounted on the NASA/U.S. Army Rotor Test Apparatus, with the rotating pitch links replaced by hydraulic actuators. These actuators generated high-frequency, low-amplitude blade pitch inputs. Individual blade pitch inputs included sinusoidal 2/rev, 3/rev and 6/rev. Additionally, multi-frequency inputs allowed for blade pitch changes at discrete azimuth locations. The Acoustic Survey Apparatus was used to acquire acoustic data with two microphones in a horizontal plane below the advancing side of the rotor. A fixed microphone recorded acoustic data aft of the rotor on the retreating side. The typical acoustic signature consisted of one strong BVI event and several smaller, secondary events. Acoustic data for the rotor without individual blade control inputs and data with inputs were compared for variations in sound pressure level.

For the microphone locations examined, reductions and increases in BVI noise occurred as a function of the type of input and the phase at which they were applied. Noise reductions were attributed to reductions in a primary BVI event, which contained most of the energy. For one microphone location on the advancing side, a maximum 7 dB reduction was measured with a 2/rev input.

Presented at the American Helicopter Society 50th Annual Forum, Washington, D.C., May 11-13, 1994. 

## Notation

| | |
|---|---|
| AMP | maximum amplitude of individual blade control input, deg |
| $A_i$ | amplification of fundamental frequency i from root to tip for wavelet input |
| azim | azimuthal location of microphone with respect to rotor hub (reference 0 deg over tail), deg |
| BL-SPL | band-limited sound pressure level, the overall energy level in the range from 150 Hz to 1.5 kHz, (referenced to 20 μPa), dB |
| c | speed of sound, ft/sec |
| $C_T$ | rotor thrust coefficient, $\text{Thrust}/\pi R^2 \rho(\Omega R)^2$ |

| | |
|---|---|
| elev | elevation angle from rotor hub to microphone (positive down), deg |
| $M_{tip}$ | hover tip Mach number, $\Omega R/c$ |
| N | number of blades |
| nP | nth rotor harmonic input of the individual blade control system |
| R | rotor radius, 16.1 ft |
| r/R | radial distance from the rotor hub to the microphone, nondimensionalized by rotor radius |
| S | rotor reference area, $ft^2$ |
| SPL | sound pressure level for each discrete frequency, dB |
| V | wind tunnel velocity, knots |
| $\alpha_s$ | corrected shaft angle of attack, positive nose-up, deg |
| $\phi_c$ | individual blade control phase corresponding to maximum amplitude (0 deg blade aft, increasing counter-clockwise looking down), deg |
| $\mu$ | rotor advance ratio |
| $\theta_c$ | amplitude of individual blade control input as a function of $\psi$, deg |
| $\rho$ | density of air, $slugs/ft^3$ |
| $\sigma$ | rotor solidity, $[(N)\ (chord)]/\pi R$ |
| $\Omega$ | rotor rotational speed, rad/sec |
| $\xi_i$ | phase shift of fundamental frequency i from blade root to tip for wavelet input, deg |
| $\psi$ | rotor azimuth angle (0 deg blade aft, increasing counter-clockwise looking down), deg |

## Introduction

Rotorcraft noise has received increased attention in recent years because of the desire to operate from convenient city-center locations and because of an increased opposition to noise by the general populace. Of the many different types of noise rotorcraft generate, blade-vortex interaction (BVI) noise is among the most annoying. This noise occurs primarily in descent conditions typical of terminal approach, and during certain types of maneuvers where the wake remains near the rotor. The distinctive "slapping" sound indicative of BVI noise occurs when the tip-vortex from one blade interacts with one or more following blades.

Experimental work in both small-scale and full-scale tests quantified the causes of BVI and clarified the rotor conditions where it exists (Refs. 1-3). The major contributors affecting the magnitude and direction of BVI noise are: the vortex strength, vortex core size, and blade/vortex miss distance (Ref. 4). Also listed in Ref. 4 but not determined to be important is the blade loading of the intercepting blade. With an understanding of the where and why BVI exist, the next step was to examine ways of reducing the noise generated.

Several experiments have looked at reducing the strength of the shed vortex by modifying the blade tip. Hoad (Ref. 5) evaluated several different blade tip planforms, affecting the vortex strength and the vortex location. Brocklehurst et al. (Ref. 6) examined reductions in the vortex strength through splitting the vortex into two distinct vortices. These were successful in reducing BVI noise for some trim conditions, but were limited because the vortex could not be eliminated. To better reduce BVI noise, vortex strength, blade loading and blade/vortex miss distance must be modified. This can best be achieved through high-frequency dynamic control of the blade pitch.

A large amount of research, both experimental and theoretical, has been conducted to evaluate higher harmonic control (HHC) (Refs. 7-9). A shortcoming of HHC is that one rotor blade can not be moved without moving all blades concurrently. To overcome this limitation and allow blade pitch changes to occur in a local azimuthal range, a high-frequency dynamic system in the rotating frame is required. Individual blade control (IBC) utilizing pitch actuation in the rotating frame meets these requirements.

A test of a full-scale BO 105 rotor system with IBC was conducted at the National Full-Scale Aerodynamics Complex (NFAC) 40- by 80-Foot Wind Tunnel. This was an international program between NASA Ames Research Center, U.S. Army Aeroflightdynamics Directorate, ZF Luftfahrttechnik, DLR and Eurocopter Deutschland. The rotor system was tested on the NASA/U.S. Army Rotor Test Apparatus (RTA) which was modified with an IBC system. The primary objectives of this test were to evaluate the capability of IBC to suppress BVI noise, increase rotor performance, reduce rotor oscillatory loads, and alleviate rotor vibrations.

This report describes the test and highlights the effects of IBC on BVI noise. Comparisons of band-limited sound pressure levels (BL-SPL) for the 6th through the 40th blade passage frequencies are used to evaluate the effects of IBC on BVI energy levels. These principle comparisons are made for one microphone location below the advancing side of the rotor. For those measurements showing reductions in the BVI noise, measurements were acquired for an acoustic survey using two microphones mounted below the advancing side of the rotor. Data are also presented from one microphone mounted below the retreating side, aft of the rotor. Reference 10 presents the effects of IBC on rotor performance, oscillatory loads and rotor vibration.

## Test Description

The following describes the rotor, model, and IBC system used for this test. Additionally, the rotor trim condition for which data were acquired is discussed along with the methods used in post-test data analysis.

### BO 105 Rotor and Rotor Test Apparatus

The rotor used for this test was a four-bladed BO 105 hingeless rotor. Table 1 contains geometric parameters of the rotor design. Reference 11 discusses the rotor in more detail. Two of the blades were instrumented with strain gages and pressure taps at several radial stations. Installation in the 40- by 80-Foot Wind Tunnel of the rotor on the RTA is shown in Fig. 1.

**Table 1:**
**General characteristics of the BO 105 rotor**

| | |
|---|---|
| Type | Hingeless |
| Radius (ft) | 16.11 |
| Number of blades | 4 |
| Blade chord (ft) | 0.886 |
| Linear blade twist (deg) | -8 |
| Precone (deg) | -2.5 |
| Solidity, $\sigma$ | 0.07 |
| Reference area, S ($ft^2$) | 57.1 |
| Airfoil section | NACA 23012 |

The RTA is a specially designed test stand for operating full-scale rotors in the wind tunnels of the NFAC. Rotor performance and loads data were acquired using the RTA's static/dynamic rotor balance. References 12 and 13 discuss the capabilities of the RTA and its balance.

### IBC system

IBC was achieved by replacing the conventional rotating pitch links with individual hydraulic actuators. These actuators, built by ZF Luftfahrttechnik, applied high-frequency control inputs at the blade root in the rotating frame. Figure 2 shows the general arrangement of the actuators in the rotor system. Hydraulic fluid was sent through a hydraulic slip ring at the base of the rotor shaft, then up through the center of the shaft to the individual actuators. A conventional rotor swashplate was used to input collective, longitudinal and lateral cyclic commands required to trim the rotor to desired conditions. Control commands from the IBC computer moved the hydraulic actuators as needed for the desired high-frequency blade pitch response. Reference 14 describes the IBC hardware and the control computer system in greater detail.

Use of hydraulic actuators in the rotating frame allowed for a wide variety of blade pitch inputs to be applied at any rotor azimuth. Transducers at the blade root were used to measure the pitch inputs of the IBC actuators. Figure 3 shows the pitch input of the conventional controls required for rotor trim. Also shown in this figure are the high-frequency IBC actuator inputs (2/rev, $\phi_C$ = 55 deg, AMP = 1 deg) and the resultant blade root pitch (a summation of the conventional and IBC inputs). Sinusoidal inputs of the 2/rev, 3/rev and 6/rev harmonics were evaluated as single-frequency inputs. The 2nd through 6th harmonics were summed in a Fourier series to generate multi-frequency inputs. The IBC phase ($\phi_C$) is defined as 0 deg when blade number 1 is over the rear of the model. The phase angle $\phi_C$ increases counter-clockwise (looking down) and is a function of the type of input.

For the single-frequency inputs, the pitch input of the IBC actuators is determined using:

$$\theta_C = \mathrm{AMP} * \cos\left[\left(\mathrm{nP} * \psi\right) - \phi_C\right] \qquad (1)$$

For the multi-frequency inputs, the equations are defined in their respective sections in the Results section below.

### Test Conditions

Acoustic data were acquired for only one low-speed, high BVI noise trim condition (Table 2). This was done to assess the effects of a wide variety of IBC inputs, while remaining within time constraints.

**Table 2:**
**Nominal rotor conditions**

| Parameter | Value |
|---|---|
| RPM | 425 |
| $C_T/\sigma$ | 0.070 |
| $M_{tip}$ | 0.640 |
| $\mu$ | 0.151 |
| V | 64 knots |
| $\alpha_S$ (corrected) | 3.9 deg. |

The $\alpha_s$ listed is corrected to account for wall effects, utilizing lifting line theory. For the nominal rotor conditions, the geometric shaft angle was 2.9 deg, with a correction of 1 deg. No attempts were made to correct the data for the effects of the test stand below the rotor.

During testing, rotor speed was adjusted to maintain a constant $\mu$ and $M_{tip}$, with conventional rotor controls adjusted to minimize 1/rev flapping. The IBC system was activated once rotor trim conditions were established. For safety reasons, no changes were made to the rotor trim after the IBC system was activated. To evaluate the effects of these trim offsets on the acoustic measurements, one case was examined when the trim was reestablished after IBC was activated (2/rev, $\phi_c$ = 160 deg, AMP = 1.0 deg). For this IBC input, no discernible difference of the acoustic signatures was found between the trimmed and untrimmed conditions. For the acoustic data presented in this paper, no corrections were applied to account for these trim differences.

Several different IBC inputs were tested, including single-frequency inputs, multi-frequency inputs, and combinations of multi-frequency inputs. A complete listing of IBC inputs tested are in Table 3.

**Acoustic Measurements**

Three microphones were used to acquire acoustic data. These were 1/2-inch condenser-type microphones utilizing nose cones. Two microphones were mounted on the Acoustic Survey Apparatus (ASA) below the advancing side of the rotor and one was fixed below the retreating side. Figure 4 shows the location of the ASA and microphones relative to the rotor. The ASA is a traversing system that allows for longitudinal movement of an array of microphones. A short, horizontal strut positioned the microphones at the desired lateral and vertical coordinates. Remote control of the ASA allowed for longitudinal placement of the microphones while the rotor was operating. The positions are listed in Table 4 (in r/R, azimuth angle (azim) and elevation angle (elev) from the rotor hub). These locations were chosen to match those used in previous small-scale BO 105 testing (Ref. 15) and to maximize the physical spacing between the rotor and microphones while remaining above the tunnel boundary layer. The fixed microphone was located on the retreating side of the rotor to evaluate the effects of IBC in this area. The location is shown in Fig. 4 and listed in Table 4. This location was selected based on the availability of microphone stands. Because only one microphone was used, no attempt was made to evaluate changes in BVI directivity on the retreating side.

The microphone signals were conditioned and amplified prior to being recorded. The amplifiers had user-selectable gains to optimize signal strength during data acquisition. The signals were then recorded onto digital tape at a sample rate of 80,000 samples/sec for 30 sec. The tape recorder utilized an anti-aliasing low-pass filter set at 2[illegible] kHz. In addition to the microphone signals, a time code, 1/rev signal, 2048/rev signal and voice were acquired. The recorded data was later used for post-test data analysis.

**Table 3:**
**IBC inputs tested**

| Input Type | Phase | AMP | ASA Location |
|---|---|---|---|
| 2/rev | sweep | 1.0 deg | * |
| 2/rev | 55 deg | 1.0 deg | sweep |
| 2/rev | 55 deg | sweep | * |
| 2/rev¥ | 55 deg | 1.2 deg | * |
| 2/rev*f* | 55 deg | 1.2 deg | * |
| 3/rev | sweep | 1.0 deg | * |
| 3/rev | 240 deg | 1.0 deg | sweep |
| 3/rev | 30 deg | 1.0 deg | sweep |
| 6/rev | sweep | 1.0 deg | * |
| 6/rev | 0 deg | 1.0 deg | sweep |
| pulse | sweep | -1.0 deg | * |
| pulse | 140 deg | -1.0 deg | sweep |
| pulse | 300 deg | -1.0 deg | sweep |
| wavelet | sweep | -1.0 deg | * |
| wavelet | 140 deg | -1.0 deg | sweep |
| wavelet | 300 deg | -1.0 deg | sweep |
| wavelet | sweep | 1.0 deg† | * |
| wavelet | 210 deg | 1.0 deg† | sweep |
| wavelet | sweep | -1.0 deg† | * |
| wavelet | 140 deg | -1.0 deg† | sweep |
| wavelet comb. | 60 & 120 deg | 1.0 deg & -1.0 deg | * |
| wavelet comb. | 60 & 120 deg | 1.0 deg & -1.0 deg | sweep |
| wavelet comb. | 60 & 120 deg | -1.0 deg & 1.0 deg | * |
| wavelet comb. | 60 & 120 deg | 1.0 deg & 1.0 deg | * |

¥ rotor thrust sweep
*f* rotor cyclic trim sweep
† wavelet pulse at blade tip had 90 deg wide base
* Location D shown in Fig. 4

**Data Analysis**

Post-test data analysis was performed using a personal computer and the Acoustic Laboratory Data Acquisition/Analysis System (ALDAS) program. Discussion of the use and options of ALDAS are in Refs. 16 and 17. The PC utilized a 12-bit analog-to-digital board to acquire data from the digital tape. An analog low-pass filter set at 5 kHz was used for anti-aliasing during post-processing.

Two different methods were used for digitizing the acoustic data from each microphone. The first method generated synchronously averaged time histories and the

second method generated frequency spectra. The time histories were used to evaluate the location and relative magnitudes of the BVI events. The frequency spectra were used to compare the acoustic energy levels for the different IBC inputs.

**Table 4:**
**Microphone locations relative to rotor hub**

| | azim | elev | r/R |
|---|---|---|---|
| Mic #1, Location A | 163 deg | -32 deg | 2.20 |
| Mic #2, Location A | 155 deg | -31 deg | 2.29 |
| Mic #1, Location B | 160 deg | -36 deg | 2.00 |
| Mic #2, Location B | 152 deg | -34 deg | 2.09 |
| Mic #1, Location C | 152 deg | -45 deg | 1.65 |
| Mic #2, Location C | 141 deg | -42 deg | 1.76 |
| Mic #1, Location D | 133 deg | -57 deg | 1.39 |
| Mic #2, Location D | 122 deg | -50 deg | 1.52 |
| Mic #1, Location E | 90 deg | -65 deg | 1.29 |
| Mic #2, Location E | 90 deg | -55 deg | 1.43 |
| Mic #1, Location F | 47 deg | -57 deg | 1.39 |
| Mic #2, Location F | 58 deg | -50 deg | 1.52 |
| Mic #3 | 317 deg | -36 deg | 1.45 |

Averaged time histories were digitized from the raw recorded data, triggering off the 1/rev signal and averaged over 40 revolutions. For a nominal rotor speed of 425 RPM, the sample rate was 14,507 samples/sec, based on 2,048 samples/rev. During this test, the rotor RPM was found to be very steady which resulted in BVI events consistently occurring within ± 2 samples over the 40 revolutions. This ensured that the averaged data was an accurate representation of the dynamic BVI.

For time history data acquired on the advancing side, digital high-pass filtering (150 Hz) was applied to remove blade loading noise. Figure 5 shows averaged data without and with the digital high-pass filter. This filter setting was found to best remove the blade loading contribution while minimizing effects on the BVI waveform. Filtering the low-frequencies from the time history data was required because for some of the test conditions, the blade loading noise was found to be a large part of the acoustic energy. This made it difficult to evaluate the time histories for those IBC inputs where the BVI noise was largely eliminated.

For the retreating-side time history data presented in this paper, no high-pass filtering was done. This was to ensure that the BVI waveform on this side was not altered by filtering. Unlike advancing side BVI, BVI on the retreating side contained more energy in the lower rotor harmonics (primarily the 5th).

Frequency spectra were determined using 4 data sets, each consisting of 8 rotor revolutions, triggered off the 1/rev. A FFT analysis (using a Hanning window) was applied to each of the 4 sets, which were then averaged in the frequency domain. This resulted in spectra with a nominal bandwidth of 1.77 Hz/line. From the frequency spectra, the energy content of the acoustic signals were determined by calculating the band-limited sound pressure level (BL-SPL). The summation procedure is:

$$BL\text{-}SPL = 10\log\left(\sum_{f=A\ Hz}^{1500\,Hz} 10^{(SPL/10)}\right) \qquad (2)$$

Where A = 150 Hz for the advancing side acoustic data and A = 100 Hz for the retreating side acoustic data.

This BL-SPL value was used as a comparative index for the different IBC inputs. This metric was chosen over conventional A-weighted dB levels because the frequency range where BVI dominates is emphasized. Figure 6 is a frequency spectrum of advancing side BVI data for the baseline BO 105 rotor. This shows the frequency band for which the BL-SPL's were determined. Below 150 Hz, blade loading noise dominates, with the majority of the energy in the first and second blade passage frequencies. The broadband noise in this range is dominated by wind tunnel noise. Between 150 Hz and 1.5 kHz the traditional scalloped shape associated with strong BVI is clearly evident, with amplitudes 10 to 20 dB above the broadband noise. Above 1.5 kHz, the BVI becomes obscured by the wind tunnel broadband noise.

For one case, low-frequency data is presented showing the effects of IBC on blade loading noise. Comparisons were made using the energy levels of the first three rotor harmonics (summing energy of the peaks plus 3 bins on each side). This minimized the effects of tunnel drive harmonics and eliminated any background noise. For this case, changes in the energy levels reflected primarily changes in the first rotor harmonic, which was 15 dB above the second and third harmonics.

## Results

Acoustic data were acquired for the nominal rotor condition (Table 2), except where noted. Advancing side BVI data presented were acquired at a principle microphone location (microphone #1 at location D), with the exception of the ASA sweeps which are outlined in Fig. 4. This principle microphone location was chosen because it contained the largest peak-to-peak values for the primary BVI event encountered in the baseline condition (no IBC). Comparisons of the data are made for the baseline case (no IBC) and for cases with single- and multi-frequency IBC inputs. The primary comparisons are through changes in the BL-SPL and examinations of the time histories. Additionally, changes in the BVI directivity are discussed for some of the IBC inputs.

### Baseline BO 105

In order to understand the effects of IBC on BVI noise, data for the baseline BO 105 rotor is first examined.

Figure 7 shows band-pass filtered time history data for the advancing side. Six pulses of differing magnitudes (labeled 1 through 6) are presented in this plot, with most of the acoustic energy in pulse #2. Pulses #5 and #6 may not be BVI, but may be reflections of the earlier events off the model. The corresponding frequency spectrum was shown in Fig. 6, with a BL-SPL of 113.2 dB.

For data on the retreating side, Fig. 8 shows a one-quarter averaged time history. There is one primary BVI pulse (labeled A), and four smaller pulses (labeled B through E). A shaft angle sweep conducted for the baseline rotor indicated that maximum level was encountered at $\alpha_S = 6.9$ deg (compared to 3.9 deg for the advancing side). For the nominal rotor conditions, the frequency spectrum is shown in Fig. 9 (corresponding to Fig. 8). This contains low-frequency blade loading noise (primarily the first rotor harmonic) and diminished BVI noise, with a BL-SPL of 114.8 dB. Note the greater amount of BVI energy in the 5th harmonic when compared to Fig. 6.

**Single-Frequency Inputs**

Single-frequency inputs are sinusoidal, with N/rev frequency. Single-frequency IBC inputs occur over the entire rotor azimuth, effecting blade dynamics over the entire disk. With IBC, all blades follow the same tracking for any N/rev input. This is different from capabilities of higher-harmonic control, where similar blade tracking is possible only for (N-1)/rev, N/rev, and (N+1)/rev inputs.

**2/Rev.** A sample IBC 2/rev input was shown in Fig. 3. For the principle microphone location, results from a $\phi_C$ sweep are shown in Fig. 10. The delta dB is the difference in the BL-SPL with and without IBC. The largest reductions occurred for $\phi_C = 55$ deg and $\phi_C = 160$ deg (7.12 dB and 7.0 dB respectively). This was the largest reduction in BL-SPL that was measured during the test. Figure 11 is a comparison of averaged time histories without and with 2/rev IBC input ($\phi_C = 55$ deg). This shows an elimination of the primary BVI events encountered for the baseline case. The reduction of the primary BVI accounts for the majority of noise reductions in all the IBC inputs tested. Unfortunately, the causes for the reduction in the primary BVI event were not conclusively determined. Whether the vortex strength, core size or blade/vortex miss distance were changed could not be determined using only acoustic data. This would require measurement of the vortex strength, core size and the blade/vortex miss distance to determine how these are being altered.

Results for the retreating side are shown in Fig. 12. For $\phi_C = 55$ deg, 2/rev IBC shows an increase in the primary BVI event as well as other, smaller events. The largest reductions in the retreating side BVI with the 2/rev input, occurred at $\phi_C = 130$ deg (4.24 dB), as shown in Fig. 13. Looking at Fig. 10, a reduction in BL-SPL was measured on the advancing side with $\phi_C = 130$ deg. Although not a maximum, this does show simultaneous reductions on both the advancing and retreating sides.

In addition to a sweep of $\phi_C$ with the 2/rev IBC, an AMP sweep and a $C_T/\sigma$ sweep were conducted at $\phi_C = 55$ deg. Figure 14 shows the variations in BVI on the advancing side, for the baseline case and with AMP = 0.4 deg, 0.8 deg, and 1.2 deg. A large decrease in the primary BVI event occurs with just 0.4 deg of input. Larger reductions occur for 0.8 deg input, but with no further reductions for 1.0 deg (Fig. 11) and 1.2 deg amplitude. For the 2/rev input, large actuator inputs are not necessary to achieve significant BVI reductions.

Moderate thrust sweeps (± 10 percent $C_T/\sigma$) for the rotor system showed little effect on the capability of the 2/rev input to reduce BVI noise (Fig. 15). The change in temporal location of the primary events are most likely due to changes in the rotor trim, not reset to zero flapping while IBC was active.

**3/Rev.** A 3/rev single-frequency input was also tested (Fig. 16). For the principle microphone location on the advancing side, this resulted in a delta dB = 5.5 dB and 6.8 dB for the BL-SPL at $\phi_C = 67$ deg and $\phi_C = 117$ deg, respectively. The time histories for both cases are shown in Fig. 17, compared with the baseline. The magnitudes of all the BVI events are reduced, although additional secondary BVI events occur. The large reductions in BL-SPL are a result of the reduction in the primary BVI event.

**6/Rev.** The 6/rev input represented the highest single-frequency evaluated during this test. A sweep of phase angle $\phi_C$ is shown in Fig. 18 (for the principle microphone location), with maximum reductions occurring at $\phi_C = 0$ deg and 20 deg (4.2 dB and 3.39 dB respectively). Time histories for the baseline, $\phi_C = 0$ deg and 20 deg are shown in Fig. 19. The advancing side BVI events were moderately reduced in magnitude. These reductions may be due to reduced vortex strength, core size, or increased blade/vortex miss distance. The temporal shift seen here is due to changes in the location of the vortex and/or changes in the location of interaction.

Note that the majority of the noise reduction occurs when the primary BVI event, which occurs at a specific azimuth location, is reduced. BVI noise reductions could be achieved by altering each blade at a discrete azimuth location, to alter or avoid the primary BVI event. This was the goal of the multi-frequency IBC inputs.

**Multi-Frequency Inputs**

The multi-frequency inputs combined 2/rev through 6/rev sinusoidal inputs to generate specific blade pitch schedules. These included single pulses, single wavelets and double wavelets. These are unique to IBC because the

resultant blade pitch can be applied at specific azimuth locations, allowing inputs tailored to specific BVI events.

**Pulse Inputs.** Pulse inputs generate a blade pitch pulse as measured at the blade root. A typical IBC actuator movement for a pulse input is shown in Fig. 20, where the maximum amplitude of the pulse occurs at the specified phase angle. The blade root input of the actuator is determined from:

$$\theta_c = \sum_{i=2}^{6} AMP_i * \cos\left[nP_i * (\psi - \phi_c)\right] \qquad (3)$$

The value of $AMP_i$ varies according to Table 5 and was given a negative value to generate a pulse with negative amplitude. Note that all frequencies are in phase.

A sweep of $\phi_C$ is presented in Fig. 21 for pulse input with negative AMP (for the principle microphone location). The largest reduction in BVI noise (4.9 dB) occurred between $\phi_C$ = 330 deg and 350 deg. A second phase angle showed a slightly lower reduction, 3.0 dB at $\phi_C$ = 90 deg. Figure 22 shows a time-history trace for one-quarter revolution of the baseline and the pulse input with negative AMP ($\phi_C$ = 90 deg and 350 deg). For $\phi_C$ = 350 deg, a reduction in the magnitude of the primary BVI event and virtual elimination of all other events occurred. For $\phi_C$ = 90 deg, the primary BVI event was reduced by half, but an earlier BVI event increased, limiting the noise reduction.

Effects of the pulse on the measured retreating side BVI are shown in Fig. 23, with a 5.7 dB reduction at $\phi_C$ = 190 deg. The corresponding acoustic time history for $\phi_C$ = 190 deg is presented in Fig. 24. The primary event is nearly eliminated, with increases in magnitude of the earlier events. Again, most of the reduction in BL-SPL occurred because of the reduction in the primary BVI event.

**Wavelet Inputs.** As discussed above, pulse inputs generated a specific blade pitch schedule at the blade root. The pitch at the blade tip will have a different pitch schedule due to blade dynamics. The wavelet input attempted to generate a specific pitch schedule at the blade tip. Figure 25 shows the calculated influence of blade dynamics on the blade pitch from the root to the tip for a wavelet input. Blade tip accelerometer data was used to determine the blade root pitch schedule necessary to achieve the desired blade tip motion. The IBC actuator inputs for a wavelet input are described using:

$$\theta_c = \sum_{i=2}^{6} \frac{AMP_i}{A_i} * \cos\left[\left(nP_i * \{\psi - \phi_c\}\right) - \xi_i\right] \qquad (4)$$

The values for $AMP_i$, $A_i$, and $\xi_i$ are listed in Table 5. $\xi_i$ represents a phase shift between the nP inputs.

It should be noted that the actual blade tip motion was not precisely known, and that using the tip accelerometers to back out the required input may have resulted in non-optimum selection of $\phi_C$ or AMP. However, because of the potential for the inputs to reduce BVI at specific azimuth angles, an exploratory matrix of test conditions were examined.

**Table 5:**
**Definitions for multi-frequency inputs**

| i | $AMP_i$ | $A_i$ | $\xi_i$ |
|---|---|---|---|
| 2 | 0.249 deg | 0.62 | -19.6 deg |
| 3 | 0.229 deg | 0.64 | -49.0 deg |
| 4 | 0.203 deg | 0.34 | -189.3 deg |
| 5 | 0.175 deg | 0.20 | -224.4 deg |
| 6 | 0.144 deg | 0.11 | -201.3 deg |

The variation in BL-SPL for the wavelet input as a function of $\phi_C$ is shown in Fig. 26 (for the principle microphone location). The largest reductions on the advancing side occurred at $\phi_C$ = 130 deg and 310 deg (3.53 dB and 3.67 dB respectively). A comparison of the time histories for the baseline and wavelet inputs with $\phi_C$ = 130 deg and 310 deg are shown in Fig. 27. The principle effect of the wavelet input was to sharply reduce the magnitude of the primary BVI event. Note that the BL-SPL reductions were limited because a secondary event preceding the primary BVI increased in magnitude.

The single wavelet inputs tested were not as effective at reducing the BVI noise as the single-frequency inputs or the single pulse inputs.

**Mixed wavelet inputs.** In addition to single wavelet inputs, a combination wavelet was used to reduce advancing side BVI by simultaneously affecting the vortex interception and vortex generation events. Figure 28 shows estimated vortex trajectories for the BO 105 rotor at the nominal rotor conditions. The primary BVI occurs at $\psi$ = 60 deg, while the associated vortex is generated at $\psi$ = 120 deg. Reducing the BVI noise at these specific locations involved wavelet inputs which generated two blade tip pulses. The first pulse had a maximum blade tip amplitude at $\psi$ = 60 deg, and the second had a maximum at $\psi$ = 120 deg. Time histories of the baseline and the combination wavelet inputs are shown in Fig. 29. Amplitude variations are defined as +/-, -/+ or +/+, corresponding to the sign of AMP for the $\psi$ = 60 deg and $\psi$ = 120 deg inputs respectively.

For the advancing side, the largest reduction in noise (3.51 dB) occurred for the +/- combination (Fig. 29b), evident by the reduction in peak-to-peak magnitude of the primary BVI event. Although the +/+ combination showed

similar reductions in the peak-to-peak levels of the primary BVI event (Fig. 29c), several secondary BVI events were introduced, resulting in less noise reduction (1.42 dB) when compared to the +/- combination. The -/+ combination (Fig. 29d) showed reductions in the BVI energy levels (2.58 dB) due to a reduction in the primary BVI event, but limited by increases in secondary events.

As with the single wavelet inputs, the use of the blade tip accelerometers may have resulted in non-optimum selection of $\xi_i$ and $AMP_i$. However, for this preliminary evaluation, the reductions in the primary BVI event that did occur suggests that the inputs were applied near the desired $\phi_c$.

**BVI Directivity**

Using the ASA, two microphones were traversed in a horizontal plane below the advancing side of the rotor to examine the changes in BVI directivity caused by different IBC inputs. Figure 4 and Table 4 presented the locations where data were acquired (labeled A through F). The contour plots in Figs. 30-33 present the BL-SPL (dB) for the physical plane traversed by the microphones, without corrections to normalize radial distance. The baseline BO 105 data is shown in Fig. 30. This figure shows a maximum BL-SPL parallel to the rotor hub (in the acoustic plane), decreasing in strength fore and aft.

Figure 31 shows the BL-SPL contour for a 2/rev input ($\phi_c$ = 55 deg). This shows a shift in the location of measured maximum level from parallel to the rotor hub to aft. For the aft locations, only slight BL-SPL reductions occurred (0.5 dB). Parallel to, and forward of, the rotor hub, reductions of 5 dB to 7 dB were measured.

Traverse sweep data for two pulse inputs with negative AMP are shown in Figs. 32 and 33 ($\phi_c$ = 140 deg and 300 deg, respectively). When compared with baseline data (Fig. 30), These show little or no reduction aft of the rotor hub. Parallel to the rotor hub, reductions of 3 to 5 dB were measured, while at the extreme forward location of the microphones, 2 to 4 dB reductions occurred.

Figure 34 shows a traverse sweep of the low-frequency 2/rev data with $\phi_c$ = 55 deg. This shows that for the physical area data were acquired, the noise pattern shifted the maximum measured level from parallel to (in the acoustic plane) the rotor, to the forward limit. This also shows a reduction of 8 dB in the maximum level measured. This low-frequency data was acquired in the near field for a localized area on the advancing side. The effects of IBC on these low-frequencies in-plane with the rotor may or may not have seen similar changes.

## Recommendations

The strength of the vortex, the vortex core size, and the blade/vortex miss distance are pieces of information that are missing from the data set. Without this inform
the effect of IBC on vortex strength, core size
blade/vortex miss distance can not be determ
Simultaneous flow visualization would hel
determining the blade/vortex miss dista
Measurements of the vortex core size should be acqui

To expand the functionality of the IBC system, a cl
loop control system could optimize reduction
acoustics and vibrations and possibly improve
performance.

## Conclusions

An international program evaluated the effects
individual blade control (IBC) on blade vortex interac
noise. Acoustic data were recorded for a range of I
inputs at a trim condition known to generate high B
noise. IBC inputs included single-frequency 2/rev, 3/re
and 6/rev. In addition, multi-frequency inputs (summat
of 2/rev through 6/rev inputs) including single pulse
single wavelets and double wavelets with positive a
negative magnitudes were evaluated.

The following conclusions can be drawn from this study:

1) For the principle microphone location on the
advancing side, IBC inputs reduce the BVI energy level
A maximum reduction of 7 dB was achieved for th
single-frequency 2/rev input.

2) For the single-frequency and multi-frequency IB
inputs tested, no single phase angle produced larg
reductions in both advancing and retreating side BV
simultaneously. Moderate simultaneous reductions i
BVI noise did occur for the 2/rev input at the principa
advancing side microphone and the retreating side
microphone.

3) Single-frequency 2/rev and multi-frequency pulse
inputs reduced BVI energy levels on the retreating side.

4) For the acoustic plane below the advancing side of the
rotor, reductions in the BL-SPL were measured parallel to
and forward of the rotor hub, with little change aft.

5) The majority of acoustic energy was determined to
exist in one BVI event. IBC inputs affecting this event
had the largest reductions in the BVI noise levels.
Secondary BVI events contained less energy, and IBC
inputs that affected these events resulted in less noise
reduction.

6) For the 2/rev input, large BVI reductions were
achieved on the advancing side with small amplitude (0.4
deg) inputs.

7) Small variations in rotor thrust (±10 percent $C_T/\sigma$) had little effect on the capabilities of the 2/rev input to reduce BVI.

8) Testing of combination wavelet inputs to reduce advancing side BVI by effecting both the vortex generation and vortex interception did not show large BVI reductions. This preliminary test may not have used the optimum phase and amplitude inputs.

9) Future efforts with IBC testing should quantify the changes in vortex strength, core size and blade/vortex miss distance.

## Acknowledgments

The authors thank Earl Booth of NASA Langley for his help in the real-time analysis of the acoustic data.

## References

1. Martin, R. M., Splettstoesser, W. R., Elliott, J. W. and Schultz, K.-J., "Advancing-Side Directivity and Retreating-Side Interactions of Model Rotor Blade-Vortex Interaction Noise," NASA TP 2784, AVSCOM TR 87-B-3, May 1988.

2. Martin, R. M., Marcolini, M. A., Splettstoesser, W. R. and Schultz, K.-J., "Wake Geometry Effects of Rotor Blade-Vortex Interaction Noise Directivity," NASA TP 3015, Aug. 1990.

3. Schmitz, F. H., Boxwell, D .A., Lewy, S. and Dahan, C., "Model- to Full-Scale Comparisons of Helicopter Blade-Vortex Interaction Noise," American Helicopter Society 38th Annual Forum, Anaheim, CA, May 1982.

4. Brooks, T. F., Jolly Jr., R. J. and Marcolini, M. A., "Helicopter Main-Rotor Noise," NASA TP 2825, Aug. 1988.

5. Hoad, D. R., "Evaluation of Helicopter Noise Due to Blade-Vortex Interaction for Five Tip Configurations," NASA TP 1608, AVRADCOM TR 80-B-1, 1979.

6. Brocklehurst, A. and Pike, A. C., "Reduction of BVI Noise Using a Vane Tip," AHS Aeromechanics Specialists Conference, San Francisco, CA, Jan. 1994.

7. Splettstoesser, W. R., Lehmann, G. and Van Der Wall, B., "Initial Results of a Model Rotor Higher Harmonic Control (HHC) Wind Tunnel Experiment of BVI Impulsive Noise Reduction," Fifteenth European Rotorcraft Forum, Amsterdam, The Netherlands, Sept. 1989.

8. Splettstoesser, W. R., Schultz, K.-J., Kube, R., Brooks, T. F., Booth Jr., E. R., Niesl, G. and Streby, O., "BVI Impulsive Noise Reduction by Higher Harmonic Pitch Control: Results of a Scaled Model Rotor Experiment in the DNW," Seventeenth European Rotorcraft Forum, Berlin, Germany, Sept. 1991.

9. Kottapalli, S., Swanson, S., LeMasurier, P. and Wang, J., "Full-Scale Higher Harmonic Control Research to Reduce Hub Loads and Noise," American Helicopter Society 49th Annual Forum, St. Louis, MO, May 1993.

10. Jacklin, S.A., Nguyen, K., Blaas, A. and Richter, P., "Full-Scale Wind Tunnel Test of a Helicopter Individual Blade Control (IBC) System," American Helicopter Society 50th Annual Forum, Washington, D.C., May 1994.

11. Peterson, R. L., Maier, T., Langer, H. J. and Tranapp, N., "Correlation of Wind Tunnel and Flight Test Results of a Full-scale Hingeless Rotor," American Helicopter Society Aeromechanics Specialists Conference, San Francisco, CA, Jan. 1994.

12. Norman, T. R., Cooper, C. R., Fredrickson, C. A. and Herter, J. R., "Full-Scale Wind Tunnel Evaluation of the Sikorsky Five-Bladed Bearingless Main Rotor," American Helicopter Society 49th Annual Forum, St. Louis, MO, May 1993.

13. Shinoda, R. and Johnson, W., "Performance Results from a Test of an S-76 Rotor in the NASA Ames 80- by 120-Foot Wind Tunnel" AIAA Applied Aerodynamics Conference, Monterey, CA, Aug. 1993.

14. Jacklin, S.A., Leyland, J.A. and Blaas, A., "Full-Scale Wind Tunnel Investigation of a Helicopter Individual Blade Control System," 34th AIAA/ASME/ASCE/ AHS/ASC Structures, Structural Dynamics and Materials Conference, La Jolla CA, April 1993.

15. Kube, R., Achache, M., Niesl, G. and Splettstoesser, W., "A Closed Loop Controller for BVI Impulsive Noise Reduction by Higher Harmonic Control," American Helicopter Society 48th Annual Forum, Washington, D.C., June 1992.

16. Watts, M. E., "ALDAS User's Manual," NASA TM 102381, April 1991.

17. Watts, M. E. and St. Jean, M. M., "Data Acquisition and Analysis on a Macintosh," American Helicopter Society International Specialist Meeting on Rotorcraft Acoustics and Rotor Dynamics, Philadelphia, PA, Oct. 1991.

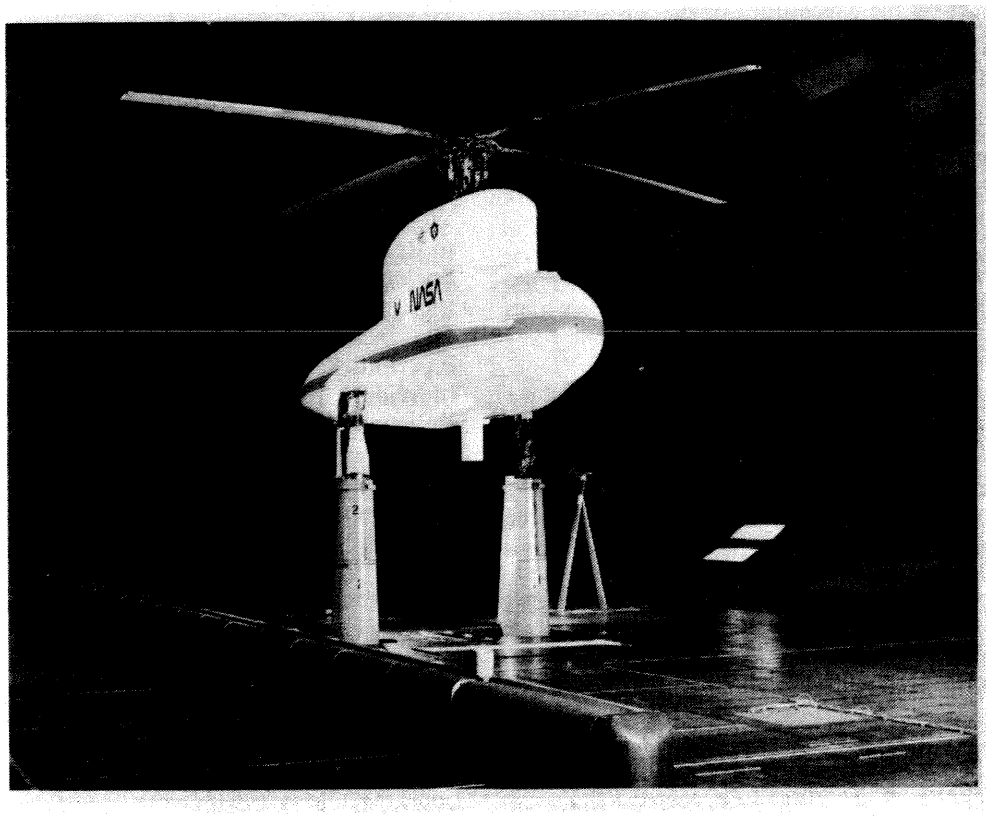

*Figure 1. Installation of RTA with BO-105 rotor and IBC system showing microphone locations.*

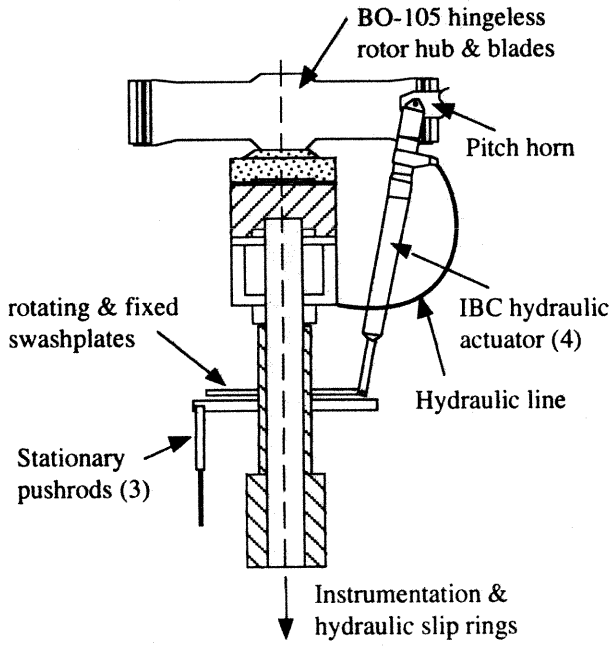


*Figure 2. Cross section of BO-105 rotor hub with IBC actuators.*

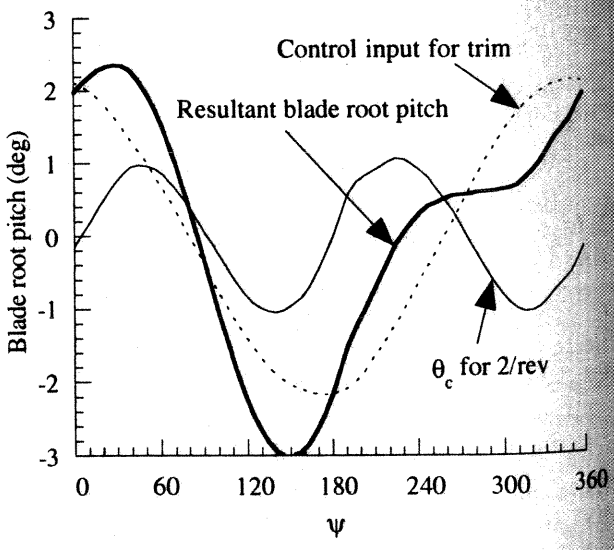


*Figure 3. Measured composition of blade root pitch inputs.*

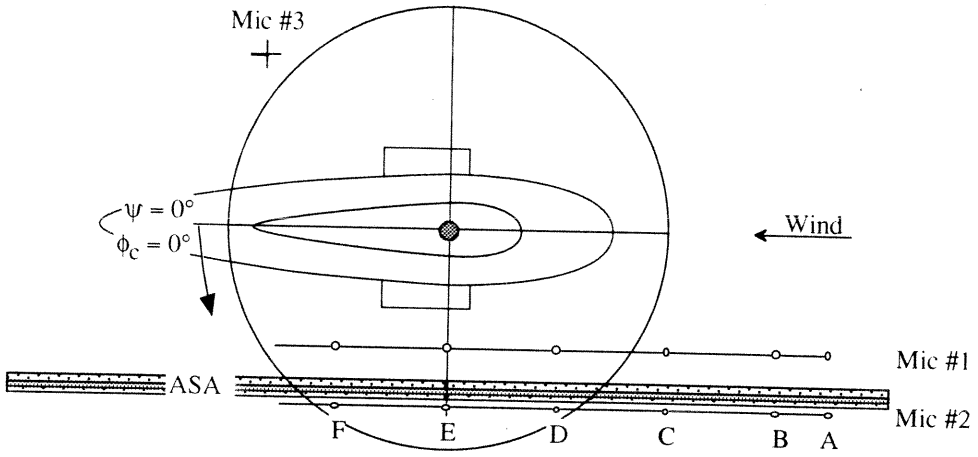


*Figure 4. General layout of microphones in 40- by 80-Foot wind tunnel.*

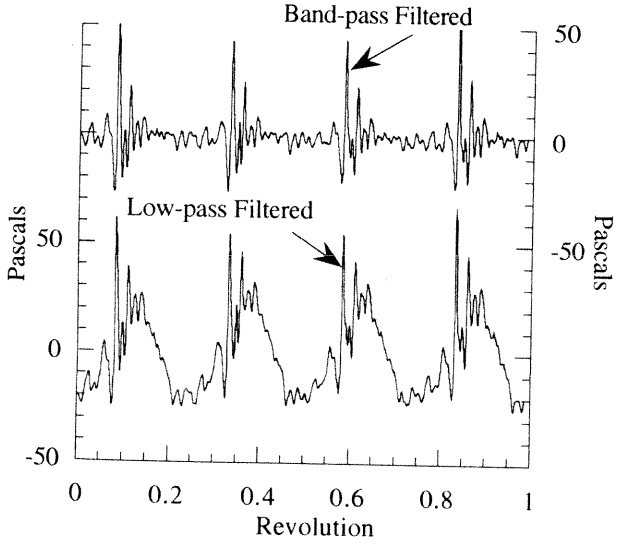


*Figure 5. Comparison of band-pass and low-pass time histories with blade loading contribution; mic #1, location D, nominal rotor conditions, no IBC.*

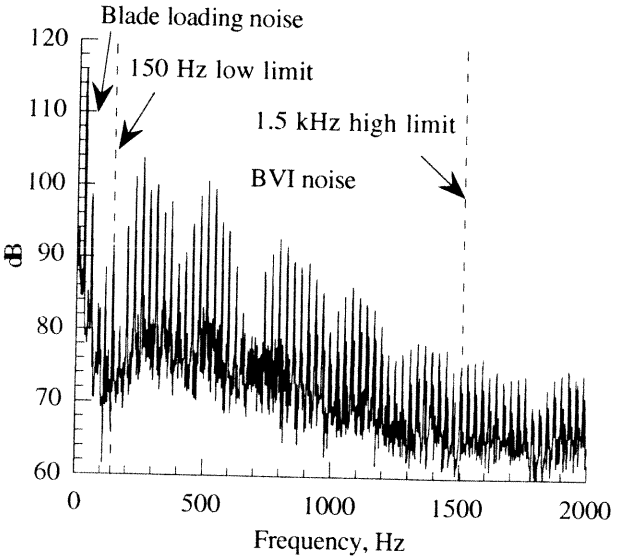


*Figure 6. Baseline frequency spectrum with blade loading and BVI noise; mic #1, location D, nominal rotor conditions, no IBC.*

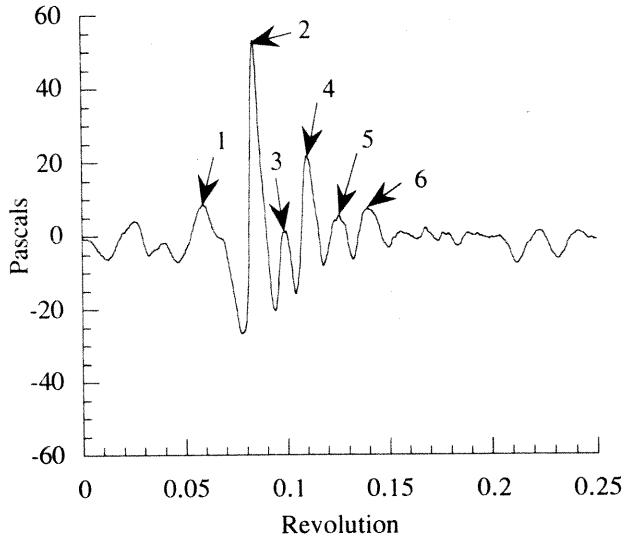


*Figure 7. Baseline time history showing BVI events; mic #1, location D, nominal rotor conditions, no IBC.*

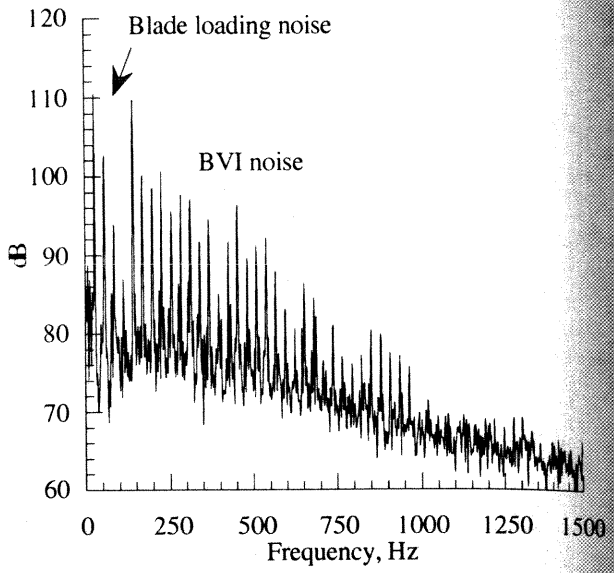


*Figure 9. Baseline retreating side frequency spectrum showing blade loading and BVI contributions; mic #3, nominal rotor conditions, no IBC.*

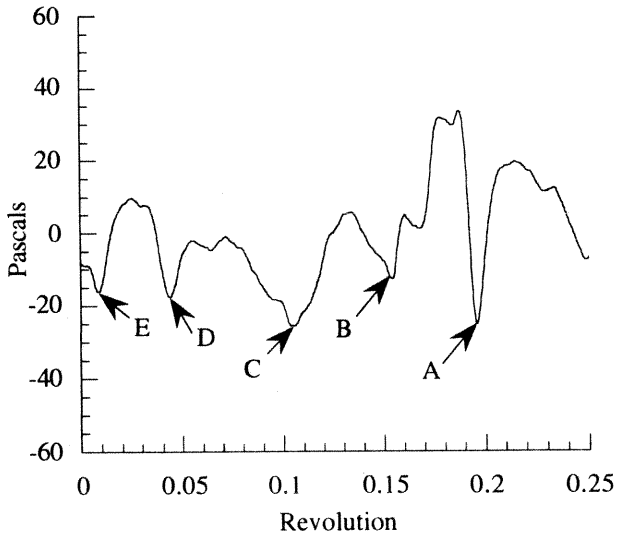


*Figure 8. Retreating side time history showing BVI events; mic #3, nominal rotor conditions, no IBC.*

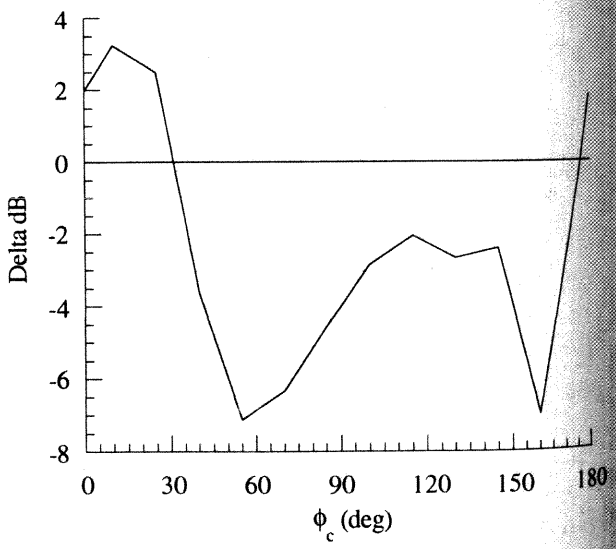


*Figure 10. Variation in BL-SPL for 2/rev IBC input compared with baseline level. mic #1, location D, nominal rotor conditions, AMP=1.0 deg.*

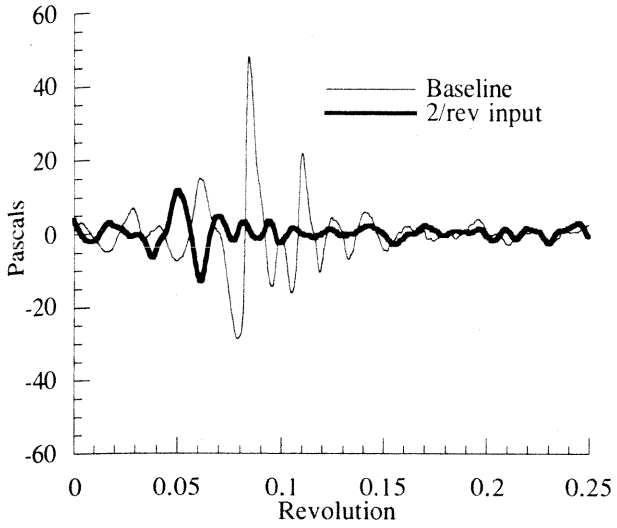


*Figure 11. Comparison of baseline and 2/rev time histories showing BVI reductions; mic #1, location D, nominal rotor conditions, $\phi_C$=55 deg, AMP=1.0 deg.*

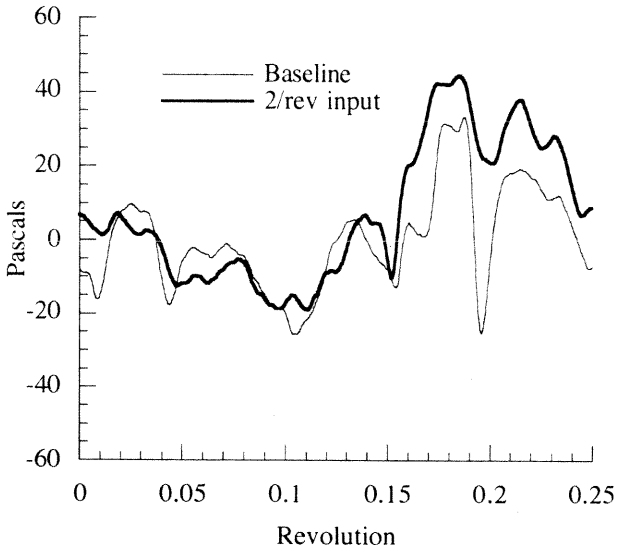


*Figure 13. Time history comparison for baseline and optimum 2/rev phase for retreating side; mic #3, nominal rotor conditions, $\phi_C$=130 deg, AMP=1.0 deg.*

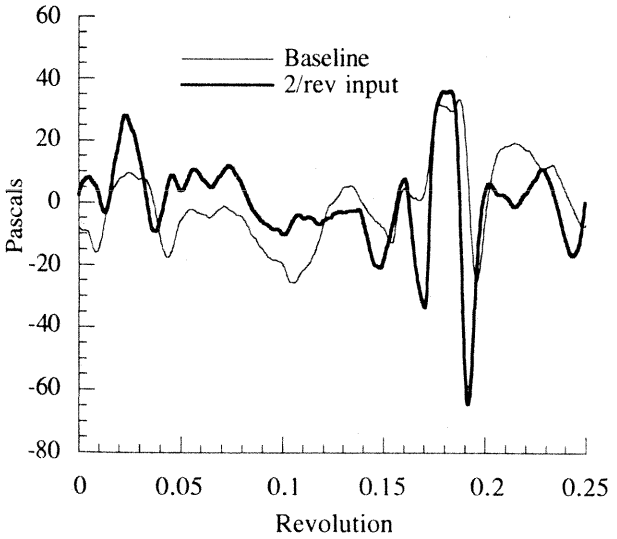


*Figure 12. Comparison of baseline and 2/rev retreating side time histories; mic #3, nominal rotor conditions, $\phi_C$=55 deg, AMP=1.0 deg.*

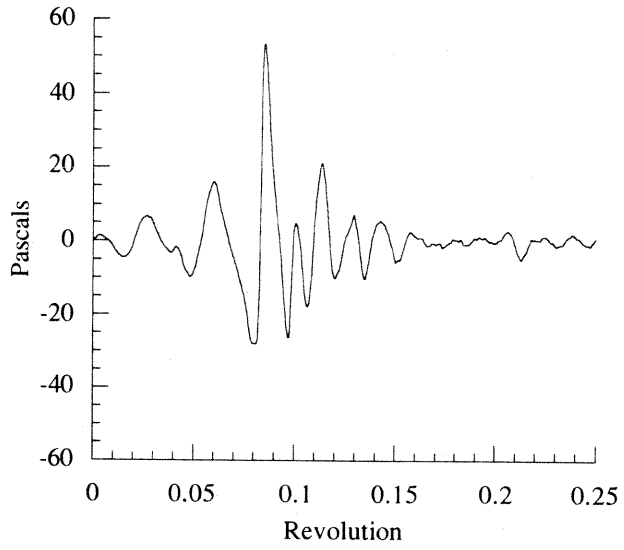


a. Baseline BVI events

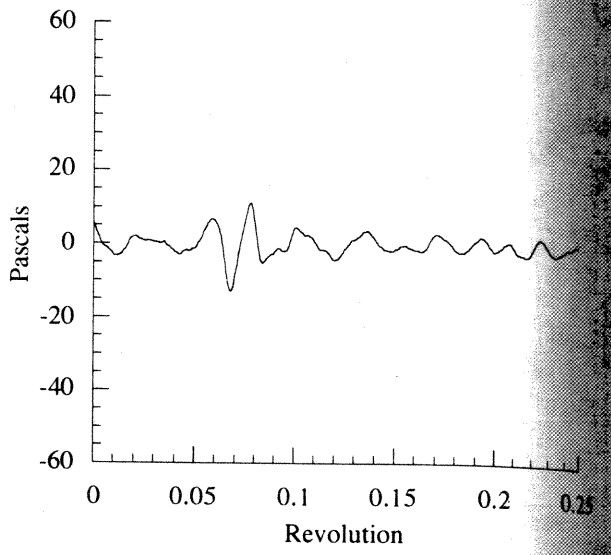


c. AMP = 0.8 deg

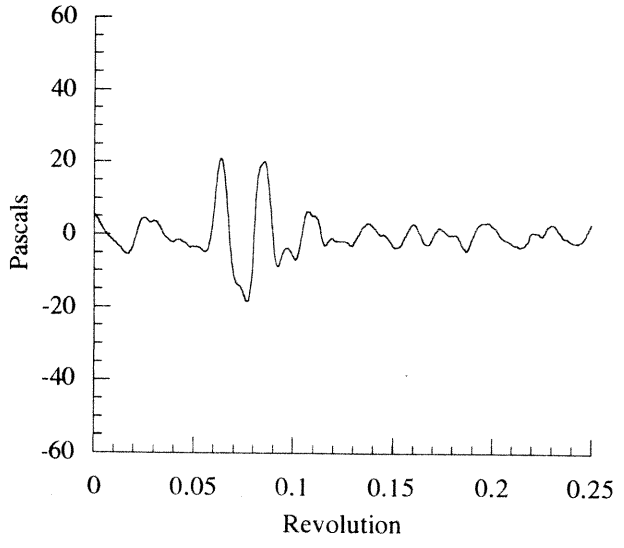


b. AMP = 0.4 deg

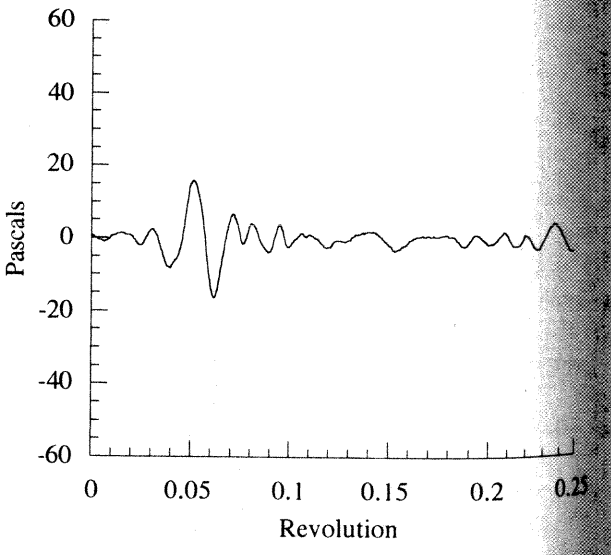


d. AMP = 1.2 deg

*Figure 14. Amplitude sweep for 2/rev IBC; mic #1, location D, nominal rotor conditions, $\phi_C$ = 55 deg.*

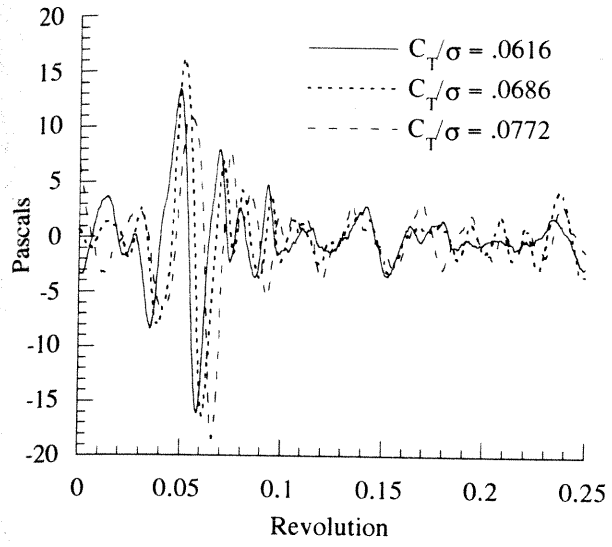


*Figure 15. Thrust sweep with 2/rev IBC; mic #1, location D, $\phi_C$=55 deg, AMP=1.2 deg.*

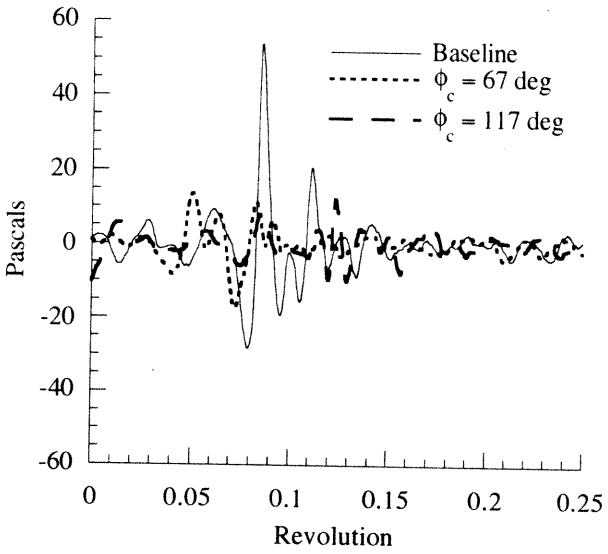


*Figure 17. Time histories for two 3/rev IBC inputs; mic #1, location D, nominal rotor conditions, AMP=1.0 deg.*

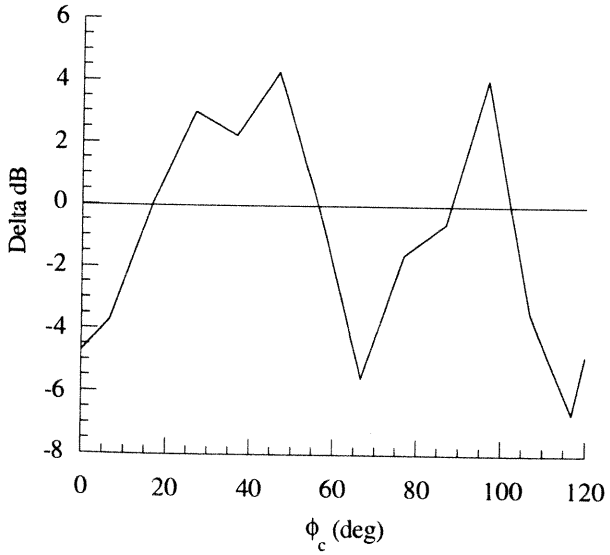


*Figure 16. Variation in BL-SPL for 3/rev IBC; mic #1, location D, nominal rotor conditions, AMP=1.0 deg.*

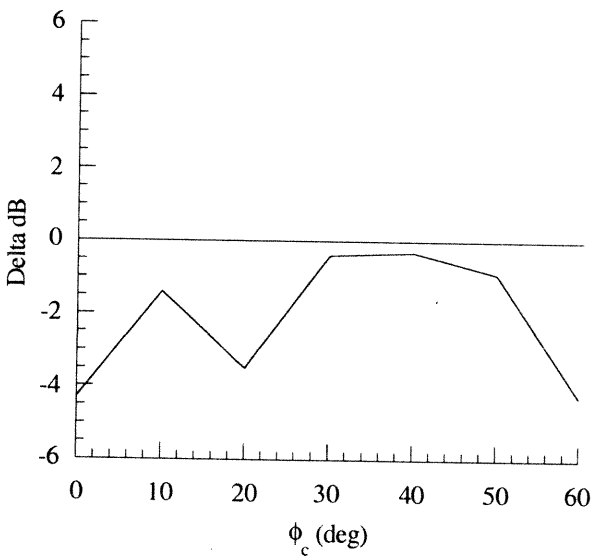


*Figure 18. Variation in BL-SPL for 6/rev IBC; mic #1, location D, nominal rotor conditions, AMP=1.0 deg.*

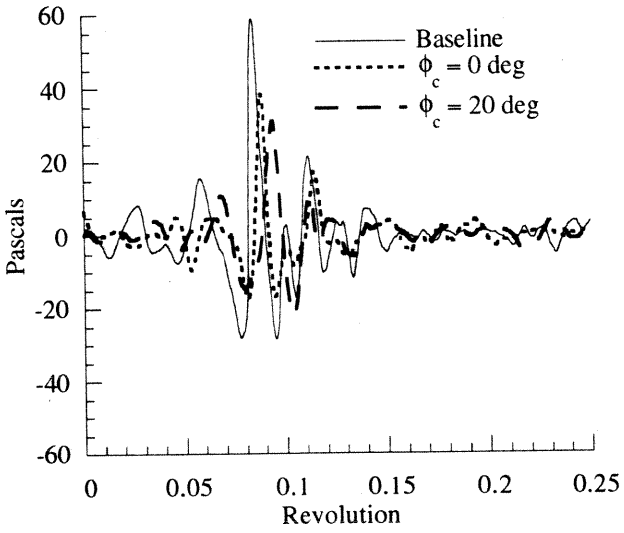


*Figure 19. Comparison of time histories for two 6/rev IBC inputs; mic #1, location D, nominal rotor conditions, AMP=1.0 deg.*

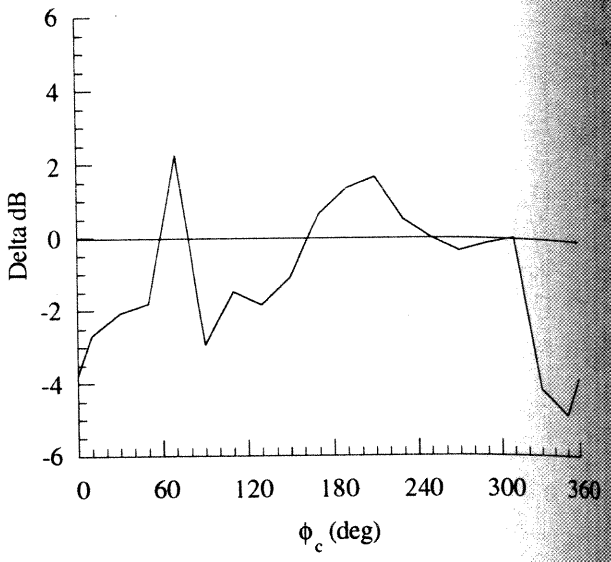


*Figure 21 Variation in BL-SPL for pulse input; mic #1, location D, nominal rotor conditions, AMP=-1.0 deg.*

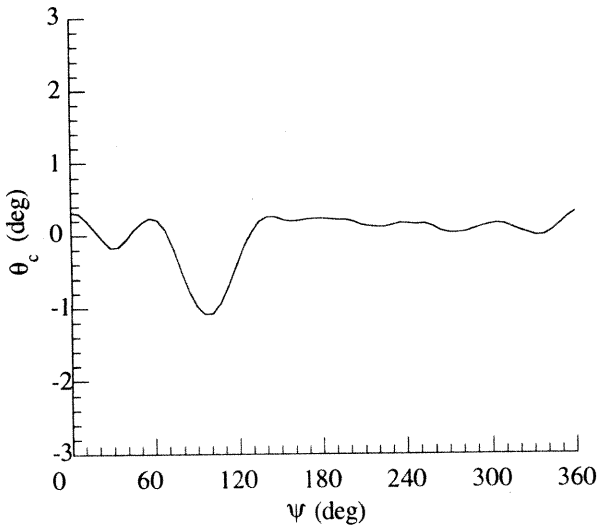


*Figure 20. Sample pulse type IBC blade root pitch input; $\phi_C$=90 deg, AMP=1.0 deg.*

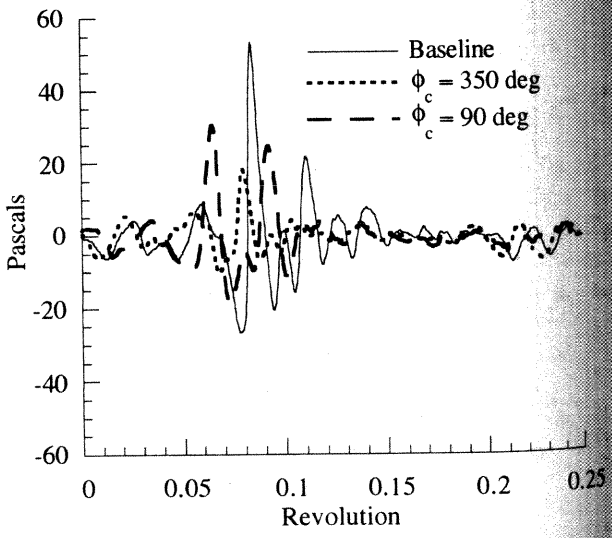


*Figure 22. Comparison of time histories for pulse input; mic #1, location D, nominal rotor conditions, AMP=-1.0 deg.*

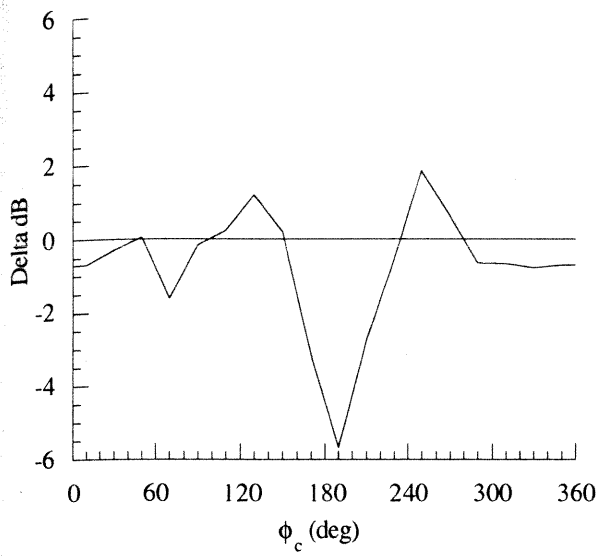


*Figure 23. Variation in BL-SPL for retreating side with pulse input; mic #3, nominal rotor conditions, AMP=-1.0 deg.*

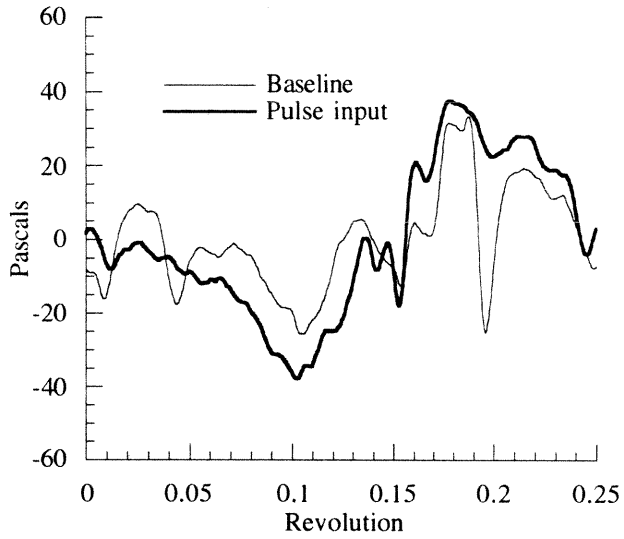


*Figure 24. Retreating side time histories for baseline and pulse input; mic #3, nominal rotor conditions, $\phi_C$=190 deg, AMP=-1.0 deg.*

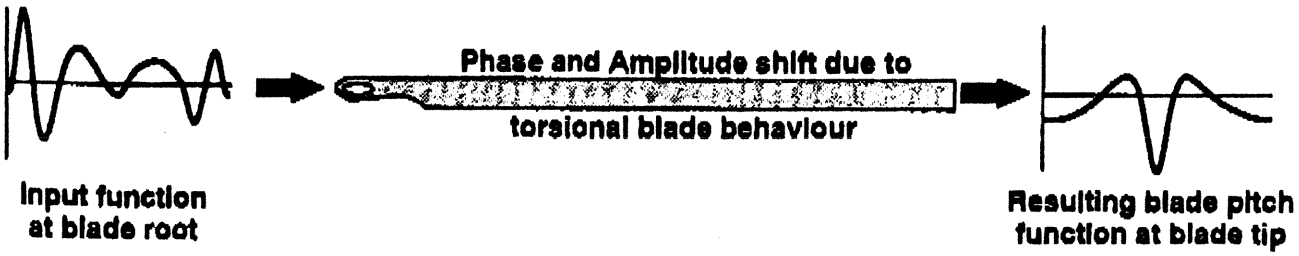


*Figure 25. Influence of blade dynamics on blade tip response; AMP=-1.0 deg.*

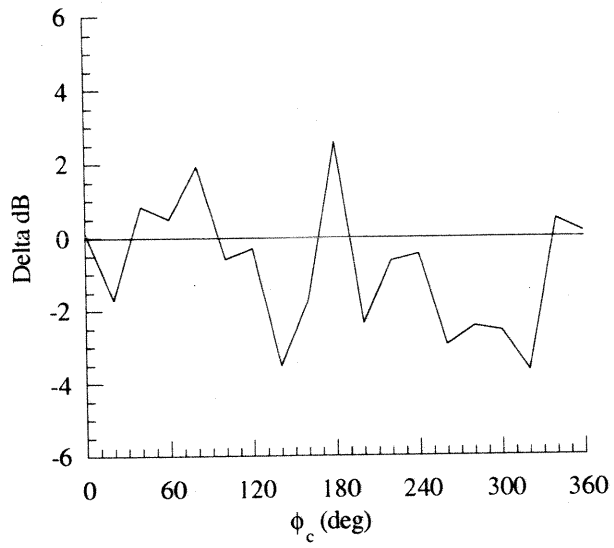


*Figure 26. Variation in BL-SPL for wavelet input; mic #1, location D, nominal rotor conditions, AMP=-1.0 deg.*

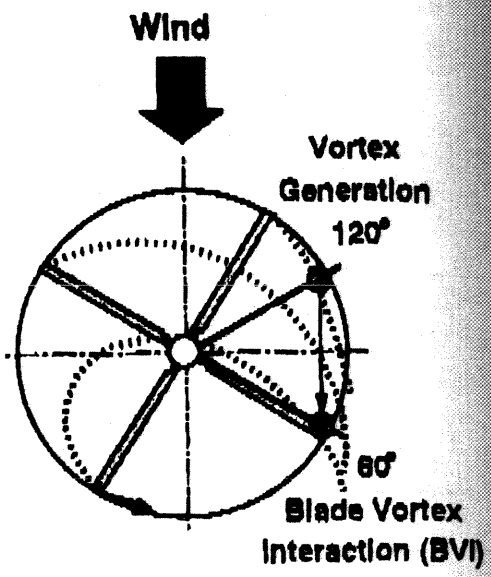


*Figure 28. Estimated locations for vortex generation and interception used for combination wavelet*

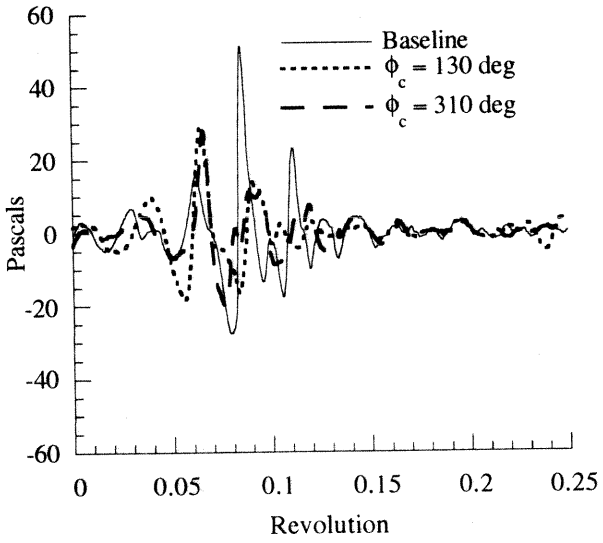


*Figure 27. Comparison of time histories of negative wavelet input; mic #1, location D, nominal rotor conditions, AMP=-1.0 deg.*

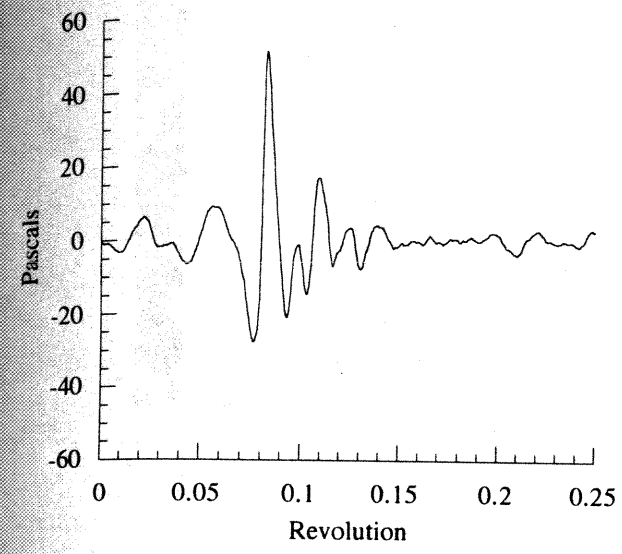


*a. Baseline time history*

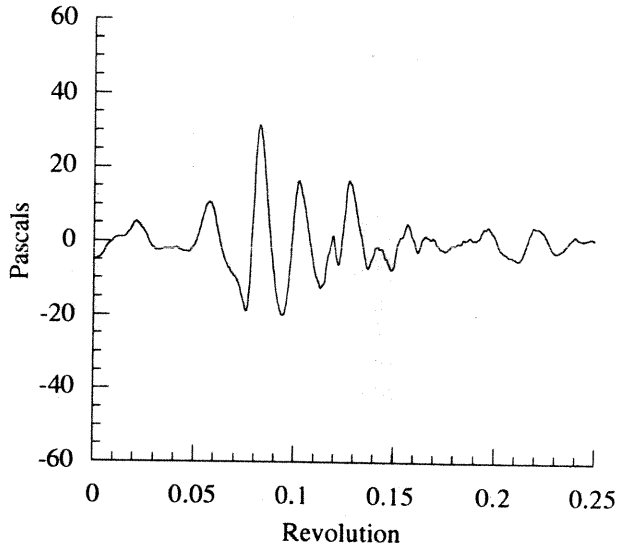


*c. AMP=1.2 deg for ψ=60 deg, AMP=1.2 deg for ψ=120 deg*

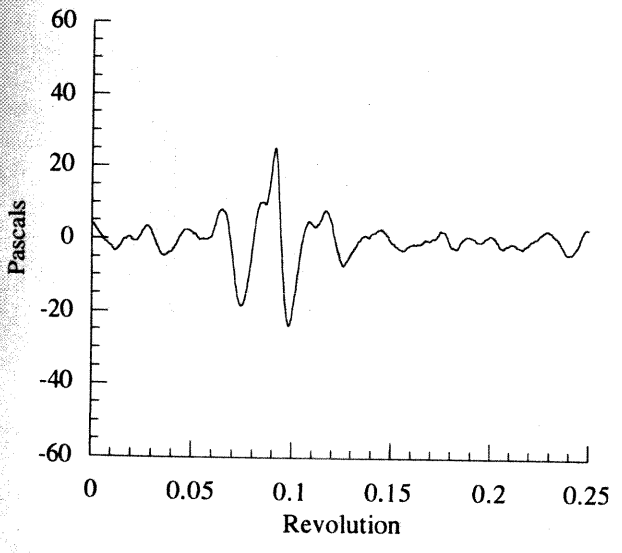


*b. AMP=1.2 deg for ψ=60 deg, AMP=-1.2 deg for ψ=120 deg*

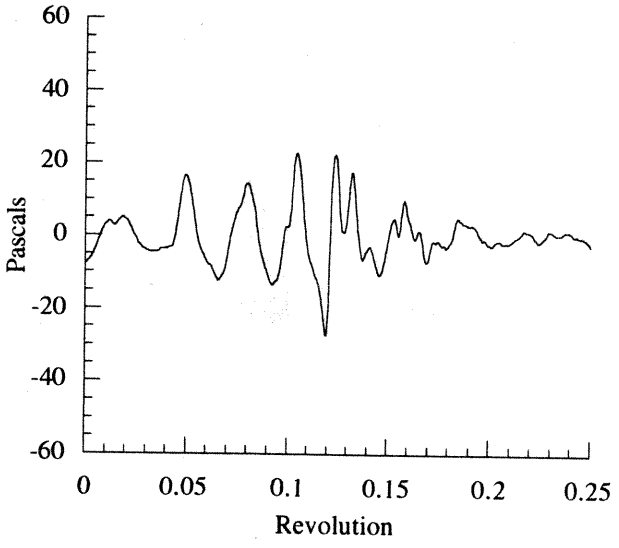


*d. AMP=-1.2 deg for ψ=60 deg, AMP=1.2 deg for ψ=120 deg*

*Figure 29. Comparison of time histories for mixed wavelet inputs with maximum amplitude at y=60 deg and y=120 deg; mic #1, location D, nominal rotor conditions.*

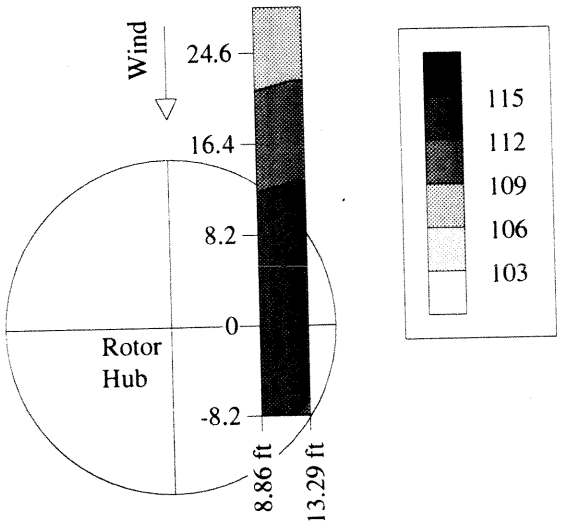


*Figure 30. Baseline BL-SPL contour plot.*

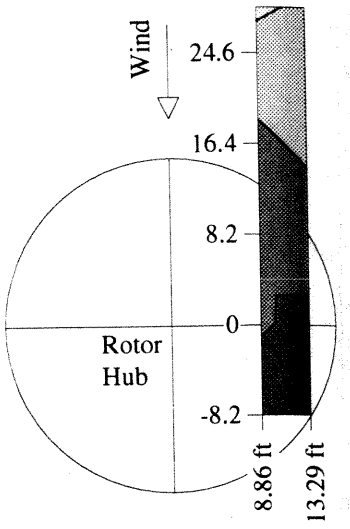


*Figure 32. BL-SPL contour for pulse input; nominal rotor conditions, $\phi_c$=130 deg, AMP=1.0 deg.*

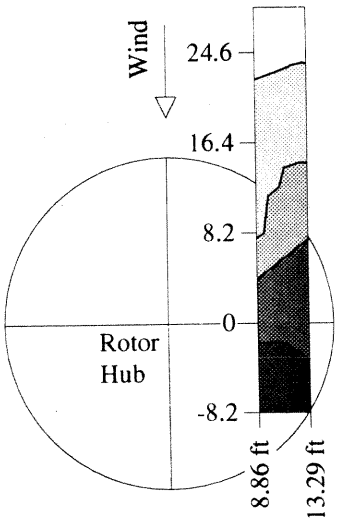


*Figure 31. BL-SPL contour for 2/rev input; nominal rotor conditions, $\phi_c$=55 deg, AMP=1.0 deg.*

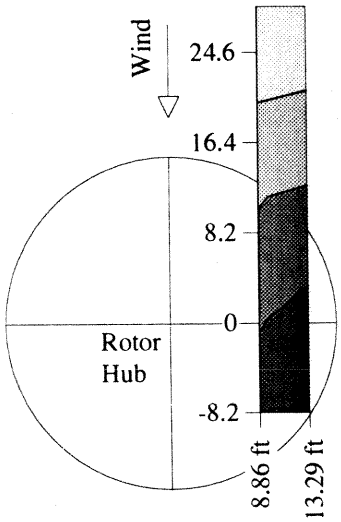


*Figure 33. BL-SPL contour for pulse input; nominal rotor conditions, $\phi_c$=330 deg, AMP=1.0 deg.*

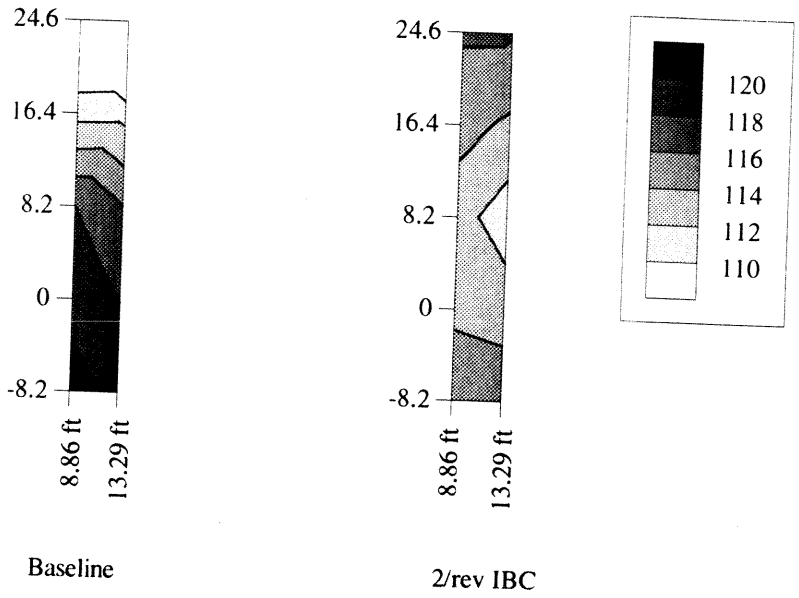


*Figure 34. Low-frequency contour for baseline and 2/rev input; nominal rotor conditions, $\phi_C$=55 deg, AMP=1.0 deg.*